Machine Vision and Applications (2006) 17(1): 21–31
DOI 10.1007/s00138-005-0012-0

ORIGINAL PAPER

Sunil K. Sinha · Paul W. Fieguth

Morphological segmentation and classification of underground pipe images

Received: 16 August 2003 / Accepted: 7 August 2005 / Published online: 18 January 2006

Abstract Visual inspection based on closed circuit television surveys is used widely in North America to assess the condition of underground pipes. Although the human eye is extremely effective at recognition and classification, it is not suitable for assessing pipe defects in thousand of miles of pipeline because of fatigue, subjectivity, and cost. In this paper, simple, robust, and efficient image segmentation and classification algorithm for the automated analysis of scanned underground pipe images is presented. The experimental results demonstrate that the proposed algorithm can precisely segment and classify pipe cracks, holes, laterals, joints and collapse surface from underground pipe images.

Keywords Segmentation · Morphology · Classification · Inspection

1 Introduction

Closed Circuit Television (CCTV) surveys are used widely in North America to assess the structural integrity of underground pipes [1]. Underground pipe scanning technology has advanced considerably during the past decade and current pipe scanners are capable of attaining very high resolutions; typical scanned images of underground concrete pipes are shown in Fig. 1. However, despite substantial progress in the *technology*, the basic means of *analysis* are unchanged: the video images in surveys are examined visually on a TV monitor and classified into grades according to the degrees of damage. Although the human eye is extremely effective at recognition and classification, it is not suitable for assessing pipe defects in thousand of miles of pipeline images due to fatigue and subjectivity, motivating the development of automated inspection systems which can assess pipe conditions to ensure accuracy, efficiency and economy. We have acquired a data set consisting of thousands of images of underground pipes from 15 major cities in North America.

The goal of our research is to develop an automated method which, given a pipe image, classifies each pixel in the image into one of five classes: background, crack, hole, joint, and lateral. In principle, after the image has been segmented into its classes, each class could be separated further into extents of distress (e.g., minor crack, major crack, multiple crack, etc.). In general, this image segmentation problem is difficult to automate because the differences between classes such as joints and cracks, although obvious to a human, can be very difficult to encode mathematically at the pixel level.

A large number of segmentation algorithms have been proposed in the literature [2, 3]. However, the literature on segmentation of defects in concrete structures is very limited. Maser [4] algorithm recommends a histogram thresholding approach, however it is not clear how the value of the threshold is originally determined. More recently, Chen et al. [5] applied a segmentation method, introduced by Kittler et al. [6], to pavement images, although the effectiveness of the method is unclear. An approach to the recognition of segmented pavement distress images is studied by Mohajeri and Manning [7], using directional filters to classify the objects. An entropy-based approach [8], which finds a bilevel threshold to maximize entropy criteria, did not improve pavement–surface images. The cluster classification process, which assigns a particular object to one of many groups by comparing typical features from each group such as a minimum distance, reported a significant amount of error [9].

In general, segmentation techniques take one of two possible approaches [10]: edge detection and thresholding. An edge is defined as the boundary between two regions with relatively distinct gray-scale characteristics, thus edge-detection techniques attempt to segment objects by outlining their boundaries. Thresholding, on the other hand, seeks to distinguish objects on the basis of their absolute intensities, for example separating a darker object from a lighter

S. K. Sinha (✉)
Department of Civil and Environmental Engineering, Pennsylvania State University, University Park, PA 16801, USA
E-mail: sunil@engr.psu.edu

P. W. Fieguth
Department of Systems Design Engineering, University of Waterloo, Waterloo, Ontario, N2L 3G1, Canada

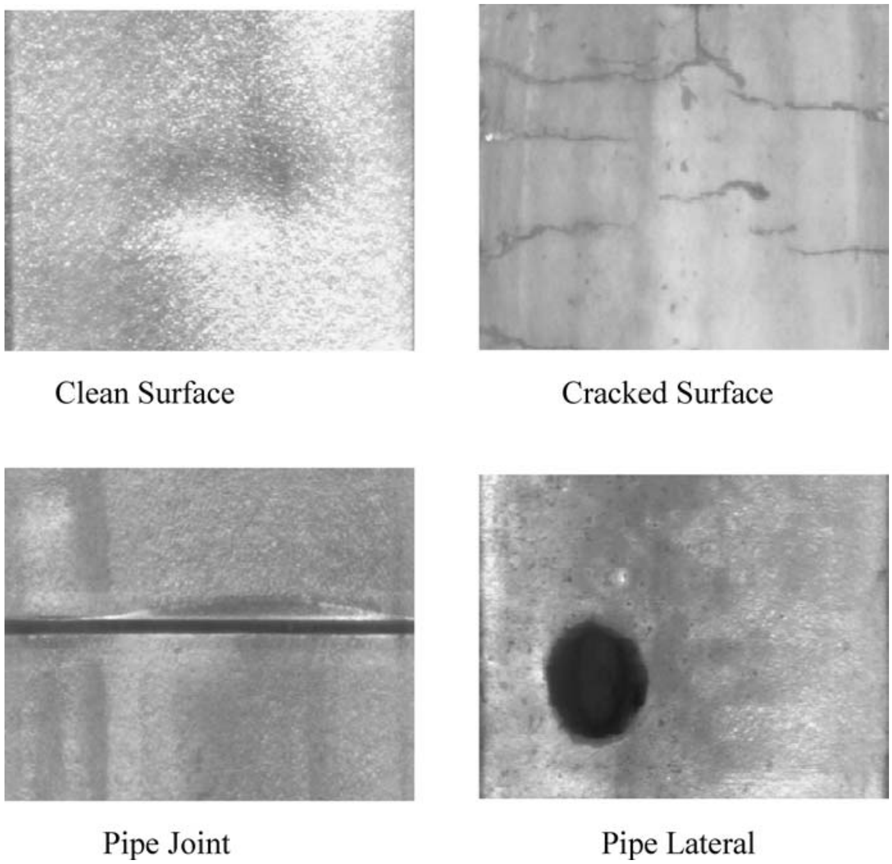

Fig. 1 Typical images of underground concrete pipe showing different objects

background, in which case a good way of segmenting might be to determine a threshold T, such all pixels with an intensity above T are classified as being part of the background.

The literature on segmentation based on gray-level intensity is inapplicable in our context since cracks, holes, joints, and laterals all appear as comparably dark objects on a lighter background, as shown in Fig. 1. Rather, it is the *geometry*, rather than the intensity, which distinguishes these objects. Mathematical morphology [11] provides an approach to the segmenting of digital images that is based on *shape*. Appropriately used, morphological operations tend to simplify images, preserving their essential shape characteristics and eliminating irrelevancies. On the basis of a formal mathematical framework, mathematical morphology is a fast, robust method that analyzes the geometry of an image directly in the spatial domain. In this paper, we develop a morphological algorithm to distinguish cracks, random background patterning, pipe joints, and pipe laterals, based on geometric criteria.

2 Image pre-processing

Since we intend to apply morphological operators, we require a grey-scale image, in which each pixel x_g is a scalar $x_g = w^T x_c$, where w is some linear projection. In the case of a two class discrimination problem, such as distinguishing between cracks and pipe background, Fisher's linear discriminant [12] can be used to determine the axis, w, onto which vector color data can be projected which preserves as much of the discriminating capability of the color information as possible. The resulting "Fisher linear discriminant" maximizes the separability of the two classes. Crack images representative of those likely to be encountered during scanning of underground pipes can be used to learn the Fisher discriminant axis using the following algorithm.

1. Calculate mean color in class $k = 1, 2$

$$m_k = \frac{1}{n_k} \sum_{x \in \chi_k} x \tag{1}$$

2. Determine the within class scatter matrices, $k = 1, 2$

$$S_k = \sum_{x \in \chi_k} (x - m_k)(x - m_k)^T \tag{2}$$

3. Find the Fisher discriminant vector

$$w = S_w^{-1}(m_1 - m_2) \quad \text{where } S_w = S_1 + S_2 \tag{3}$$

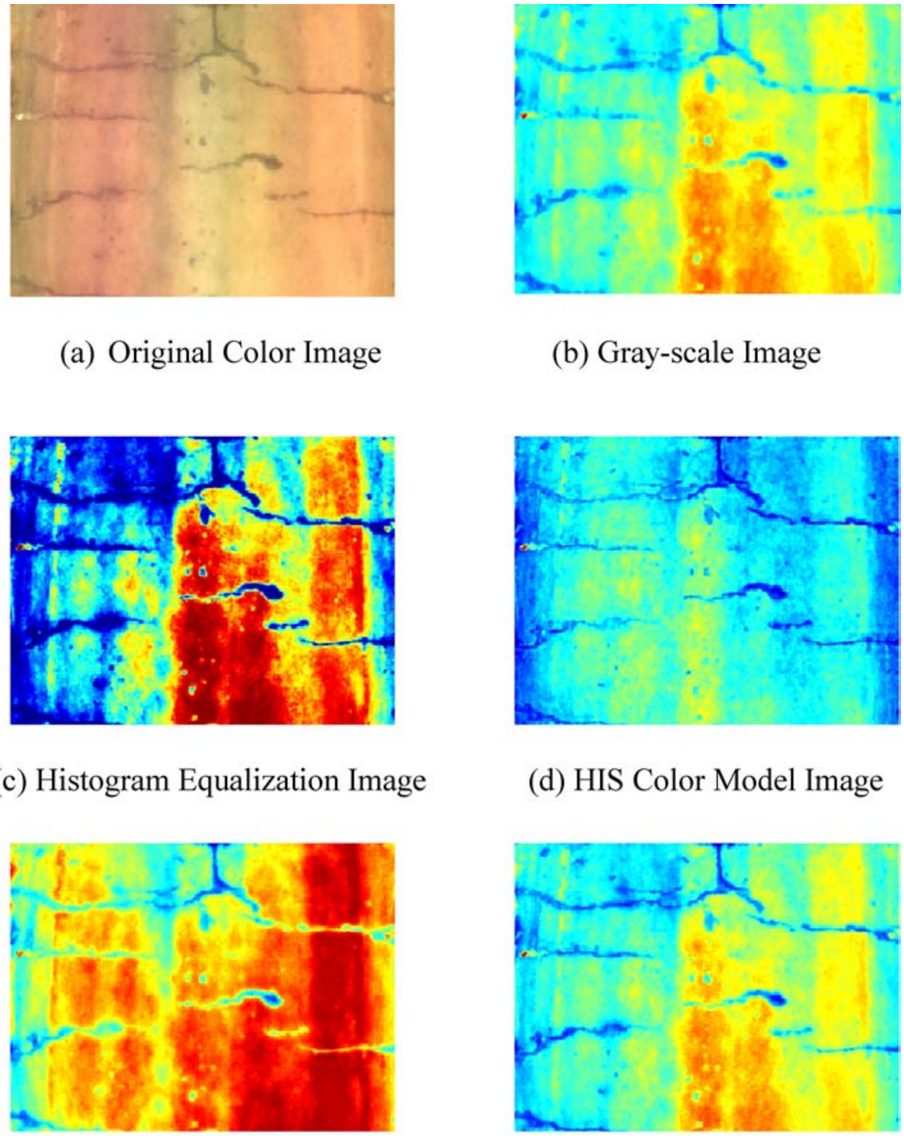

(a) Original Color Image (b) Gray-scale Image

(c) Histogram Equalization Image (d) HIS Color Model Image

(e) YIQ Color Model Image (f) Fisher Discriminant Image

Fig. 2 Fisher's discriminant analysis can be used to enhance the contrast between the pipe background and cracks. In gray-scale image (**b**) there is little contrast between the background and cracks. The Histogram equalization (**c**) enhances the contrast of image by transforming the values in an intensity image. The HIS and YIQ color models can also be used to provide additional contrast (**d**) and (**e**), respectively; although the pipe image shows high contrast, the crack boundary is blurred and the image is noisy. Projection onto a Fisher axis (**f**) enhances the contrast and enables better extraction of the crack features

Pipe images representative of those likely to be encountered during object recognition and classification can be used to learn the Fisher discriminant axis. Figure 2 shows that Fisher's discriminant analysis can be used to enhance the contrast between the pipe background and cracks. In the gray-scale image (Fig. 2b) there is little contrast between the background and cracks. The HIS and YIQ color models can also be used to provide additional contrast as shown in Fig. 2c and d, respectively; although the pipe image shows high contrast, the crack boundary is blurred and the image is noisy. The projection onto the Fisher axis (Fig. 2e) enhances the contrast and enables better extraction of the crack features.

3 Morphological segmentation and classification

Mathematical morphology [11] is a widely used methodology for image analysis. Morphology operates on image regions (e.g., the light and dark portions of an image), where the regions can be reshaped (i.e., morphed) in various ways under the control of a structuring element. The structuring element can be thought of as a parameter to the morphological operation. The most fundamental operations are morphological *dilation* and *erosion*. On the basis of these, two compound operations, *opening* and *closing*, can be defined.

In underground pipe image segmentation, the following classes are of general interest: the pipe joints (horizontal dark straight lines), pipe laterals (circular dark objects), surface cracks (irregularly shaped thin dark lines), and the pipe background (anywhere from a smooth to a highly patterned surface). The goal of our research is to segment pipe joints, laterals, and cracks based on the *geometric* differences between them, specifically based on morphology.

The premise of the morphological approach is to distinguish objects on the basis of shape. With the canonical shapes being thin and wide (joints), large and round (laterals), and small and irregular (cracks, holes), the key idea of this paper is to use two parameterized structuring elements: a circular structuring element (S_C) of radius r (Fig. 3), and a horizontal structuring element (S_H) of varying length l and fixed width $w = 3$ (Fig. 4). As the effect of an opening is to remove those features, which are small relative to the structuring element S while preserving features greater than S, the choice of these two elements (circular and rectangular) is clearly designed to mimic the geometry of the laterals and joints to be extracted. The key idea, then, is that we can isolate objects of a given "size" by performing a series of opening operations, on the basis of structuring elements of varying size. The "size" of any object can then is defined mathematically as the largest structuring element (measured here in terms of radius r or length l) that can be inscribed in the object. Note that, aside from the general shape of the structuring element, we do not make any specific assumption regarding the shape of the object being measured, therefore this definition of size is quite general and will prove effective in measuring sizes of cracks, irregular laterals, etc., which otherwise resist specific characterization. The segmentation algorithm consists of a sequence of processing steps, illustrated in Fig. 5.

0	0	0	0	0	1	0	0	0	0	0
0	0	0	1	1	1	1	1	0	0	0
0	0	1	1	1	1	1	1	1	0	0
0	1	1	1	1	1	1	1	1	1	0
0	1	1	1	1	1	1	1	1	1	0
1	1	1	1	1	1	1	1	1	1	1
0	1	1	1	1	1	1	1	1	1	0
0	1	1	1	1	1	1	1	1	1	0
0	0	1	1	1	1	1	1	1	0	0
0	0	0	1	1	1	1	1	0	0	0
0	0	0	0	0	1	0	0	0	0	0

Radius 'r'

Fig. 3 Circular structuring element, S_C

0	0	0	0	0	0	0	0	0	0	0
0	0	0	0	0	0	0	0	0	0	0
0	0	0	0	0	0	0	0	0	0	0
0	0	0	0	0	0	0	0	0	0	0
1	1	1	1	1	1	1	1	1	1	1
1	1	1	1	1	1	1	1	1	1	1
1	1	1	1	1	1	1	1	1	1	1
0	0	0	0	0	0	0	0	0	0	0
0	0	0	0	0	0	0	0	0	0	0
0	0	0	0	0	0	0	0	0	0	0
0	0	0	0	0	0	0	0	0	0	0

Width 'w'

Length 'l'

Fig. 4 Horizontal structuring element, S_H

3.1 Morphological opening and thresholding

We performed a morphological opening operation on the underground pipe image with increasing sizes of the circular and horizontal structuring elements. Clearly, as the size of the structuring element is increased features of increasing size are removed by the morphological opening. For example, a structuring element of intermediate size will preserve laterals and a collapsed pipe, but will remove cracks and small holes.

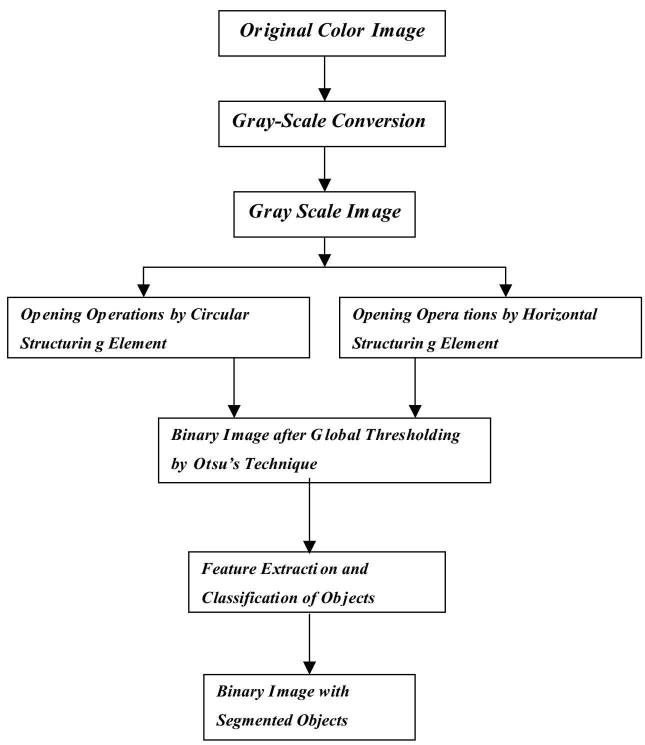

Fig. 5 Overview of the proposed morphological segmentation approach

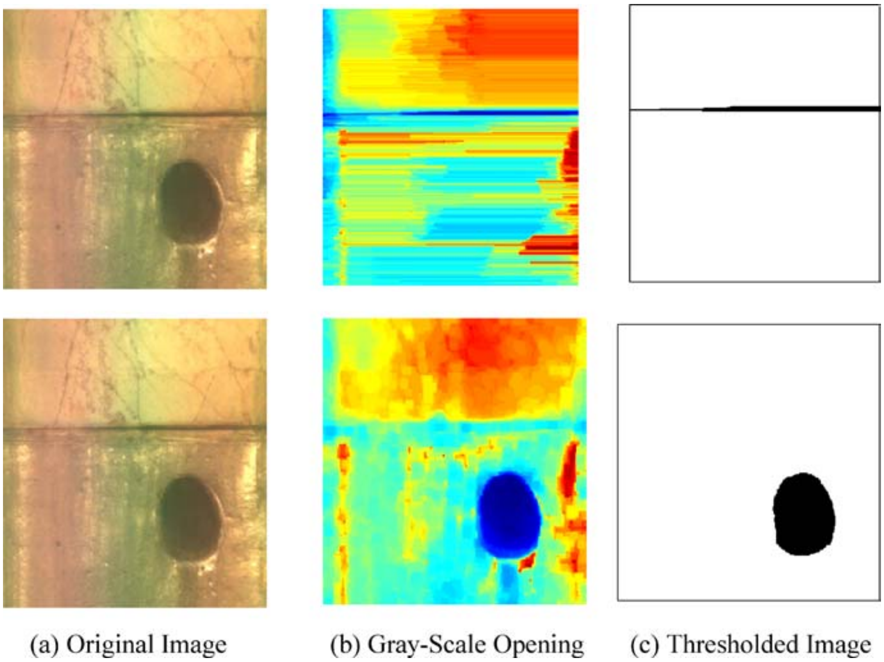

Fig. 6 This figure illustrates joint/lateral discrimination using different structuring element: a horizontal element (*top*) of length 285 mm, consistent with the geometry of a perfect joint, as opposed to a circular element (*bottom*) of radius 57 mm, tuned to the shape of a perfect lateral

Figure 6b shows two examples of the results of gray-scale opening. Although some of the original features in 6a are still clearly present, the output of the morphology is confusing and not easily interpreted. What we really want is an additional processing step, a thresholding function $t()$, classifying each pixel as

$$t(p(x,y)) = \left\{ \begin{array}{ll} 0, & \text{pixel is geometrically consistent with} \\ & \quad \text{structuring element} \\ 1, & \text{pixel is not consistent} \end{array} \right\} \tag{4}$$

That is, the set of all "dark" (zero valued) pixels will identify the object(s) in the image which are compatible (i.e., bigger than) the selected structuring element. Ideally, we would like a single global threshold "T" such that

$$t(p(x,y)) = \left\{ \begin{array}{l} 0,\ p(x,y) \le T \\ 1,\ p(x,y) \ge T \end{array} \right\} \tag{5}$$

Unfortunately, it is difficult in general to find a single threshold that is best for an arbitrary gray-scale image. Many approaches have been proposed to find an optimal threshold level for certain image cases [13, 14]. We propose to use Otsu's method [14] because it is non-parametric, unsupervised, and automatic. A discriminant criterion is computed for each possible threshold "T"; the optimal threshold is that gray-level where this measure is maximized. The results of Otsu's method are illustrated in Fig. 6c: the segmented joint and lateral stand out very clearly. With a methodology in place for understanding the results of a given morphology, we can now study the choice of structuring elements that will be most effective in classifying each pipe object. Figures 7 and 8 plot the average area of objects in each class (crack, hole, joint, etc.) based on circular and horizontal structuring elements, respectively. That is, if we let $|t(I)|$ represent the number of dark pixels in I after binary thresholding, then Figs. 7 and 8 actually plot the normalized areas

$$a_{\mathrm{L}}(r) = \frac{|t(I \circ S_{\mathrm{C}}(r))|}{|t(I_{\mathrm{L}})|} \tag{6}$$

$$a_{\mathrm{J}}(l) = \frac{|t(I \circ S_{\mathrm{L}}(l))|}{|t(I_{\mathrm{J}})|} \tag{7}$$

where I_{L}, I_{J} are idealized, prototype images of the perfect lateral and joint. Note that all of the curves are monotonically decreasing,

$$|I \circ S_{\mathrm{C}}(r_1)| \ge |I \circ S_{\mathrm{C}}(r_2)|, \quad \text{for all } r_1 \le r_2 \tag{8}$$

since a larger structuring element cannot leave more pixels in place than a smaller element. Although the plots in Figs. 7 and 8 are interesting and intuitive, in order to accurately isolate and classify different objects in an image we have to take into account the *variations* in the area of each class. That is, holes, laterals, etc., all come in a range of sizes, and this range *must* be taken into account in selecting the appropriate structuring element to serve as a classifier.

We can compute or assess the ability of any structuring element to discriminate between any two classes (e.g., crack and hole) by examining the $D_{i,j}$ degree to which two classes

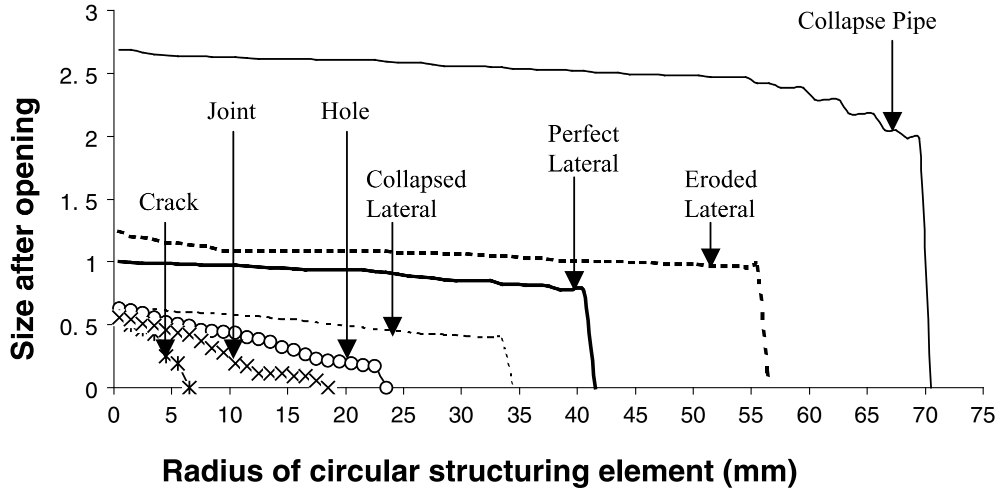

Fig. 7 Morphological analysis based on a circular structuring element: the average area of each class is plotted as a function of the structuring element diameter; area is normalized to that of an ideal lateral. Clearly, as the diameter is increased, classes with thin, elongated geometries (e.g., cracks, joints) are quickly eliminated

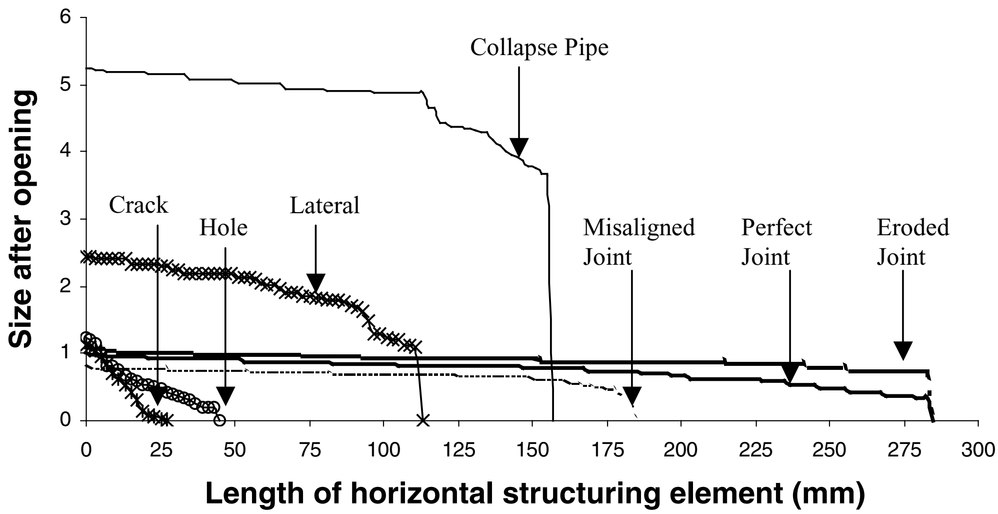

Fig. 8 Morphological analysis based on a horizontal structuring element: the average area of each class is plotted as a function of the structuring element length; area is normalized to that of an ideal joint. Clearly, as the length is increased, classes with small geometries (e.g., cracks, holes) are quickly eliminated

are separated relative to their standard deviations:

$$D_{i,j}(r) = \frac{|\mu_i(r) - \mu_j(r)|^2}{\sigma_i^2(r) + \sigma_j^2(r)} \tag{9}$$

$$\mu_i(r) = \langle a_{\mathrm{L}}(r) \rangle_i \tag{10}$$

$$\sigma_i^2(r) = \left\langle a_{\mathrm{L}}(r)^2 \right\rangle_i - \langle a_{\mathrm{L}}(r) \rangle_i^2 \tag{11}$$

where $\langle\,\rangle_i$ represents an average taken over images of class i. A parallel definition exists for discriminant $D_{i,j}(l)$ based on a horizontal structuring element. The value of r for which $D_{i,j}(r)$ is maximized represents the optimal feature by which to discriminate between classes i and j on the basis of the area (i.e., the number of pixels) remaining after a morphological opening by element $S_{\mathrm{C}}(r)$. By plotting $D_{i,j}(r)$ and $D_{i,j}(l)$ for different classes i, j we can deduce the set of features to be extracted for classification. Figures 9 and 10 plot $D_{\mathrm{L},i}(r)$ and $D_{\mathrm{J},i}(l)$ respectively, indicating peaks to identify these features.

The average morphological operations execution times for horizontal and circular structuring elements are 25 and 32 ms, respectively. All experiments are conducted on Intel Pentium Dual Processor 3.2 with 800 MHz running Matlab software.

The proposed morphological segmentation and classification algorithm will work very well for underground pipe images containing one class of object only in a given frame. In the real world problem, underground pipe images may

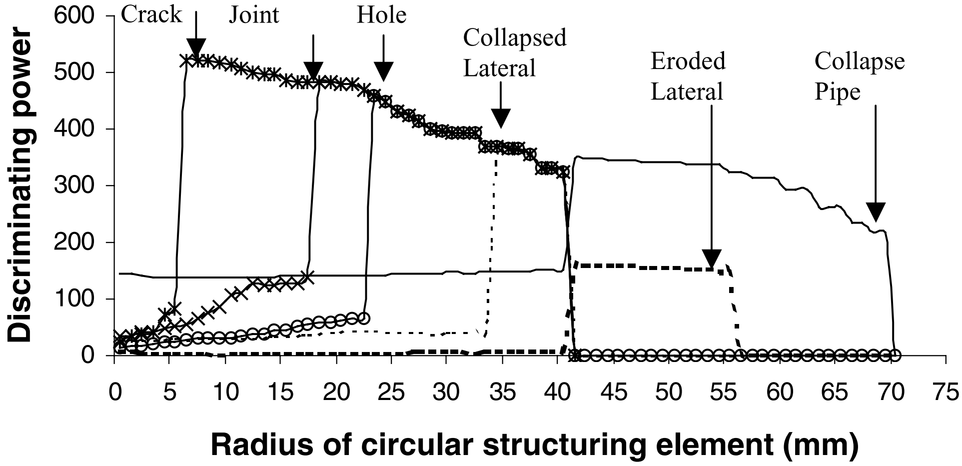

Fig. 9 Lateral discrimination: we can distinguish between laterals and other classes by opening with a circular structuring element, as in Fig. 6. We can plot the ability to discriminate "*D*" between an ideal lateral and any other class as the difference in response (normalized to standard error) to the structuring element

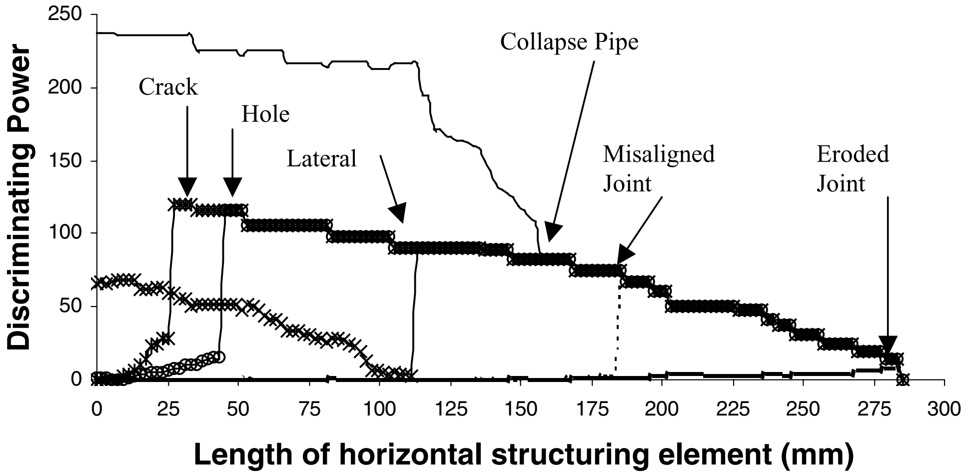

Fig. 10 Joint discrimination: we can distinguish between joints and other classes by opening with a horizontal structuring element, as in Fig. 7. We can plot the ability to discriminate "*D*" between an ideal joint and any other class as the difference in response (normalized to standard error) to the structuring element

contain cluttered objects as shown in Figs. 11a and 12a. For segmentation and classification of such images, we suggest a slightly different approach. The new approach is based on taking the difference of image after each morphological opening and thresholding operations. Figures 11c and 12c illustrate the procedure of taking difference of image after successive opening operations to segment various objects present in the image. Once the objects are segmented, then feature extraction and classification can be done.

3.2 Feature extraction and classification

The sizes of structuring elements for the classification of objects in images can be determined from the discriminant method described in the previous section. For example, if an image is opened with $S_C(2)$ – the circular structuring element of radius 2 mm – then small objects (e.g., random background patterning) are removed. By repeating this process for different sizes of elements $S_C(7)$, $S_C(23)$, $S_C(57)$, we can group objects by size, into their classes.

Specifically, we propose to keep as our features

$$a_L(r) = |t\,(I \circ S_C(r))|\,, \quad r \in \{2, 7, 23, 57\} \tag{12}$$

where the features are selected to discriminate between successive class pairs clean-pipe, cracks, holes-joints, laterals, and pipe-collapse. A further set of four features is chosen based on rectangular elements:

$$a_J(l) = |t\,(I \circ S_H(l))|\,, \quad l \in \{2, 47, 121, 155\} \tag{13}$$

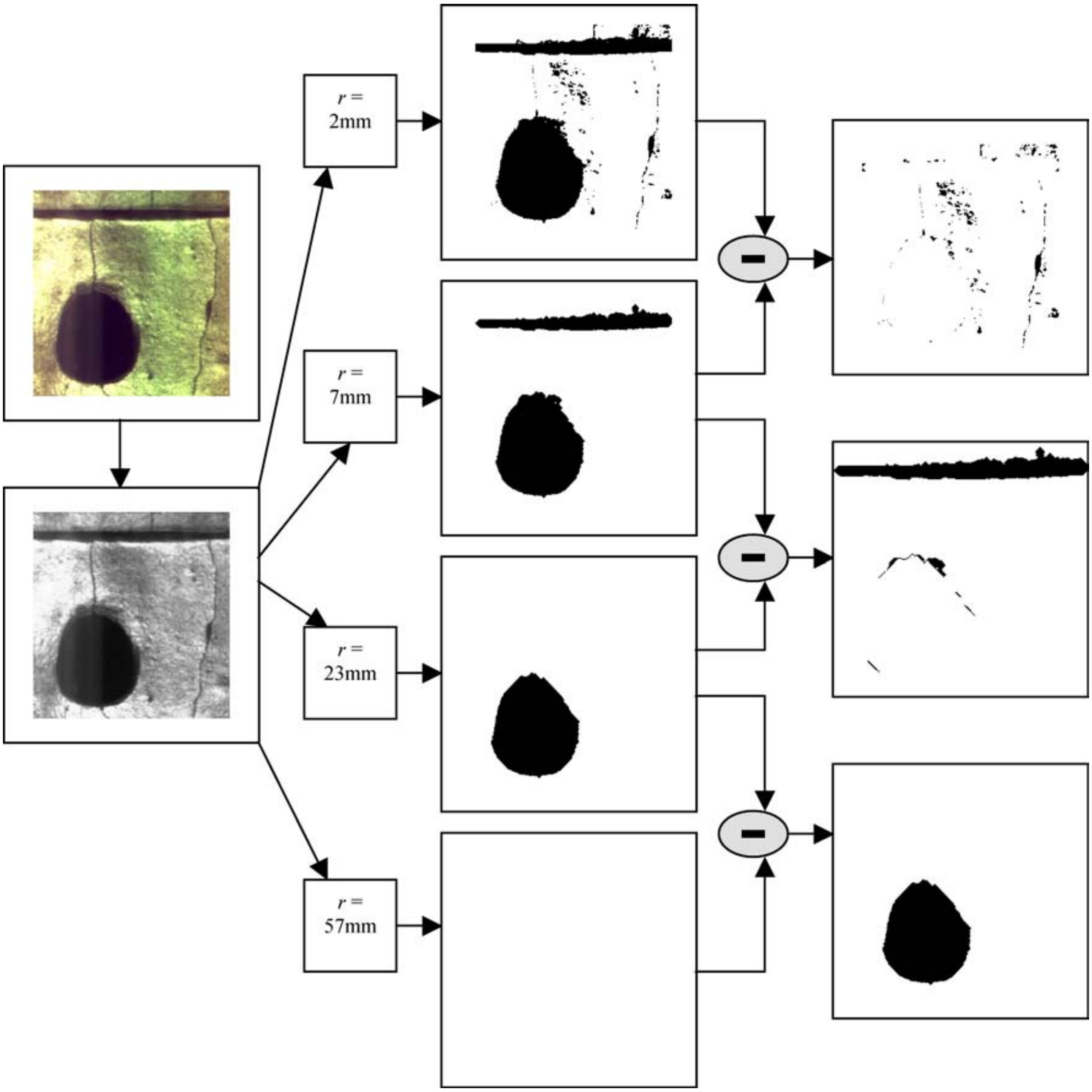

Fig. 11 Classification results by using circular structuring element: the original images are opened by structuring element of different sizes as outlined in Table 1, and finally binary images are obtained by global thresholding technique. **a** Gray-scale image; **b** thresholded images after opening operations; **c** classified images

selected to discriminate between successive pairs of clean-pipe, cracks-holes, laterals, joints, and pipe-collapse. The classifier is then made up of pairwise discriminants, such as

$$a_L(l) \underset{\text{Class 2}}{\overset{\text{Class 1}}{\gtrless}} \tau(l) \tag{14}$$

where the threshold $\tau(l)$ is based on criterion discriminating between two classes. To maximize $D_{i,j}(r)$ – the separation of the class means normalized to the standard deviations—the optimum threshold in discriminating classes i and j is the weighted mean

$$\tau_{i,j}(r) = \frac{\sigma_i(r)\mu_i(r) + \sigma_j(r)\mu_i(r)}{\sigma_i(r) + \sigma_j(r)}, \tag{15}$$

thus

$$\tau_{0,1}(r) = \frac{\sigma_{\text{crack}}(r)\mu_{\text{clean}}(r) + \sigma_{\text{clean}}(r)\mu_{\text{crack}}(r)}{\sigma_{\text{crack}}(r) + \sigma_{\text{clean}}(r)} \tag{16}$$

The deduced thresholds are listed in Tables 1 and 2 The threshold values shown in Tables 1 and 2 are selected on the basis of the pixel count area of the classified class. For example, segmented collapse pipe image will have the pixel area count of more than 1700 as compared to the segmented crack or hole in the pipe image, which will have pixel area count of less than 1700.

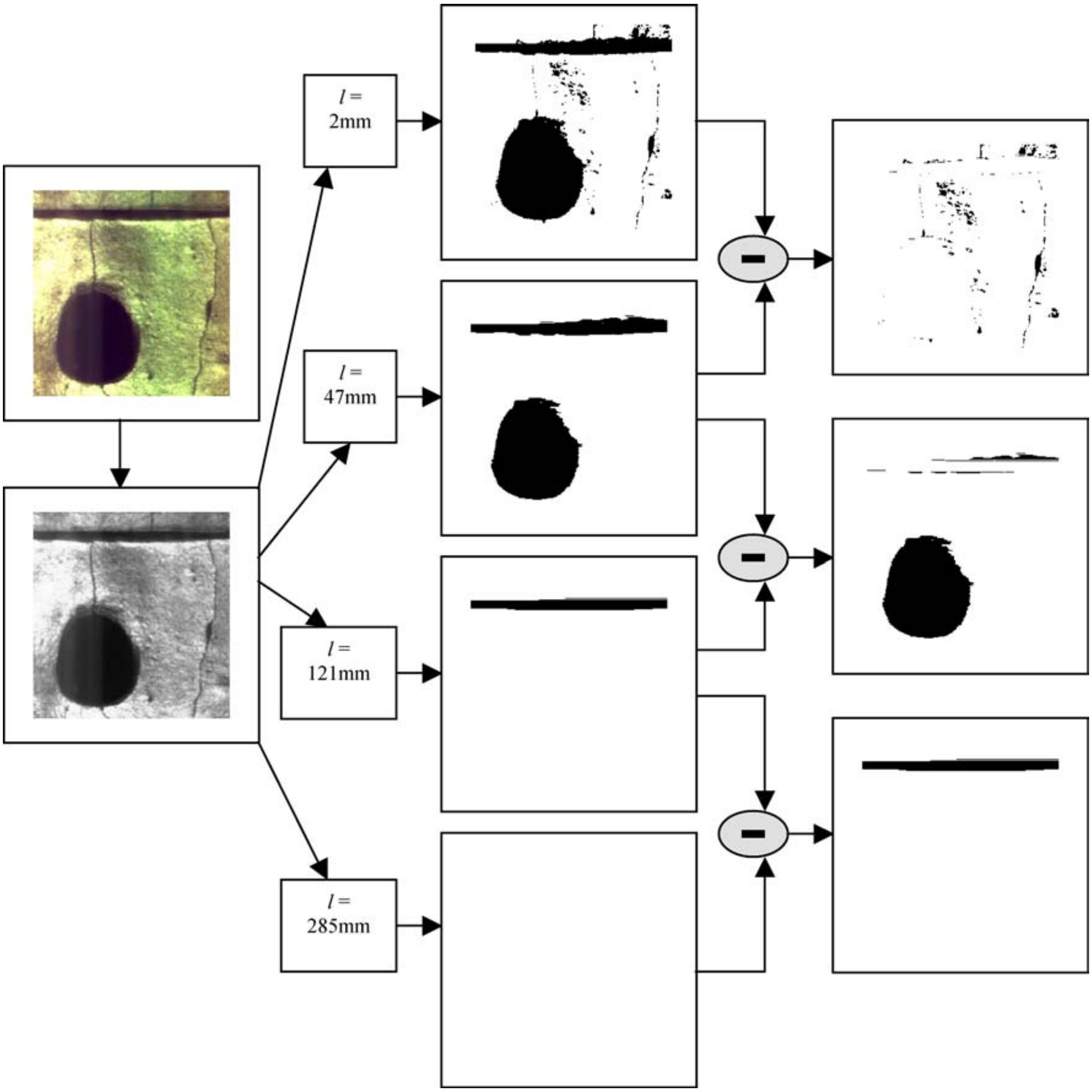

Fig. 12 Classification results by using horizontal structuring element: the original images are opened by structuring element of different sizes as outlined in Table 2, and finally binary images are obtained by global thresholding technique. **a** Gray-scale image; **b** thresholded images after opening operations; **c** classified images

4 Experimental results

We have applied the proposed approaches to 825 underground concrete sewer pipe images. These images are obtained from SSET inspection of flush cleaned concrete sewer pipes, eighteen inches in diameter, from various municipalities in North America. In this study, 500 of the images are used for training the classifiers and the remaining 325 are used to test the classifiers. The training and testing sets are randomly selected from each class of defects in the

Table 1 Appropriate threshold selected for classification of various objects in the underground pipe images by circular structuring element

Threshold values for classification by circular structuring element					
No.	$A_R(2)$	$A_R(7)$	$A_R(23)$	$A_R(57)$	Classified class
1	<150				Clean pipe
2	>150	<1000			Crack
3	>150	>1000	<1700		Hole/joint
4	>150	>1000	>1700	<3150	Lateral
5	>150	>1000	>1700	>3150	Collapse pipe

Table 2 Appropriate threshold selected for classification of various objects in the underground pipe images by horizontal structuring element

Threshold values for classification by horizontal structuring element					
No.	$A_L(2)$	$A_L(47)$	$A_L(121)$	$A_L(155)$	Classified class
1	<150				Clean pipe
2	>150	<1000			Crack/hole
3	>150	>1000	<1700		Lateral
4	>150	>1000	>1700	<3150	Collapse pipe
5	>150	>1000	>1700	>3150	Joint

Table 3 Confusion matrix using the circular structuring element as classifier (Row-Morphological classifier results and Column-Expert labeling)

Class	Clean pipe 1	Crack 2	Hole/joint 3	Laterals 4	Pipe collapse 5	Total	Percent correct
1	**50**	0	0	0	0	50	100
2	0	**85**	15	0	0	100	85
3	0	0	**95**	5	0	100	95
4	0	0	1	**47**	2	50	94
5	0	0	0	4	**21**	25	84
Total	50	85	111	56	23	325	
		Overall percentage correct classification					91.7

Table 4 Confusion matrix using the horizontal structuring element as classifier (Row-Morphological classifier results and Column-Expert labeling)

Class	Clean pipe 1	Crack/hole 2	Lateral 3	Pipe collapse 4	Joints 5	Total	Percent correct
1	**49**	0	0	0	1	50	98
2	0	**141**	0	0	9	150	94
3	0	0	**48**	0	2	50	96
4	0	0	0	**24**	1	25	96
5	0	0	0	0	**50**	50	100
Total	49	141	48	24	63	325	
		Overall percentage correct classification					96

825 image database. We may evaluate the performance of proposed segmentation and classification methods by confusion matrix indicating whether the classification tendency is reasonable or not. On the confusion matrix, if we have a normal distributed matrix with few outliers, centered on the diagonal, the classification can be said to be reasonable. Tables 3 and 4 show the agreement and disagreement between the expert classification and the proposed classifier in terms of confusion matrix for the testing set of 325 images by using circular and horizontal structuring elements, respectively.

We have also evaluated the performance of our color image pre-processing methodologies as discussed earlier in Sect. 2. The results are presented in Table 5. As shown in Table 5, the morphological classification results obtained by using Fisher Discriminant pre-processing method are much better than other standard image pre-processing methods (Gray-scale, Histogram equalization, HIS color model, and YIQ color model).

5 Conclusions

We have demonstrated a morphological approach to segment and classify images of underground concrete pipes. We assume that an image consists of five types of objects,

Table 5 Evaluation of image pre-processing methodologies

Processing methods	Morphological classifier results by circular structuring element (% Correct)	Morphological classifier results by horizontal structuring element (% Correct)
Gray-scale	77.2	82.6
Histogram equalization	65.1	62.7
HIS color model	69.8	72.2
YIQ color model	59.4	61.6
Fisher Discriminant	91.7	96

namely the crack, hole, joints, laterals and surface collapse, and we estimate their sizes on the basis of the concept of gray-scale morphological opening operations. With this size information, we provide a precise removal and classification of various objects present in an underground pipe image. Experimental results demonstrate that the proposed approach is effective for dealing with the underground pipe images with varying background pattern and non-uniform illumination. Once the laterals, joints and holes are segmented and classified from the image then the crack filters, as described in [15], can be used for precise detection of crack features.

References

1. Iseley, T., Abraham, D.M., Gokhale, S.: Intelligent sewer condition evaluation technologies. In: Proceedings of the North American NO-DIG Conference, pp. 254–265. Seattle, WA (1997)
2. Canny, J.F.: A computational approach to edge detection. IEEE Trans. Pattern Anal. Mach. Intell. **8**(6), 679–698 (1986)
3. Chen, S.Y., Lin, W.C., Chen, C.T.: Split and merge image segmentation based on localized feature analysis and statistical tets. CVGIP-Graphics Models Image Process. **53**(5), 457–475 (1991)
4. Maser, K.R.: Computational Techniques for Automating Visual Inspection. Massachusetts Institute of Technology, Report, Cambridge, MA (1987)
5. Chen, K.B., Soetandio, S., Lytton, R.L.: Distress identification by an automatic thresholding technique. In: Proceedings of the International Conference On Application of Advanced Technologies in Transportation Engineering. San Diego, CA (1989)
6. Kittler, J., Illingworth, J., Foglein, J., Parker, K.: An automated thresholding algorithm and its performance. In: Proceedings of the 7th IEEE International Conference on Pattern Recognition, pp. 287–289 (1984)
7. Mohajeri, M.H., Manning, P.J.: ARIA: An Operating System of Pavement Distress Diagnosis by Image Processing. Transp. Res. Record vol. 1311, Transportation Research Board, pp. 120–130. Washington, D.C. (1991)
8. Abutaleb, A.S.: Automatic thresholding of gray-level pictures using two-dimensional entropy. Comput. Vision Graphics Image Process. **47**, 22–32 (1989)
9. Acosta, J.A., Figueroa, J.L., Mullen, R.L.: Feasibility study to implement the video image processing technique for evaluating pavement surface distress in the state of Ohio. In: Proceedings of the Federal Highway Administration. Ames, Iowa (1992)
10. Heijden, F.V.D.: Image Based Measurement Systems. Wiley, New York (1994)
11. Sera, J.: Introduction to mathematical morphology. Comput. Vision Graphics Image Process., 283–305 (1986)
12. Duda, R.O., Hart, P.E.: Pattern Classification and Scene Analysis pp. 271–272. Wiley, New York (1970)
13. Parker, J.P.: Gray-level thresholding in badly illuminated images. IEEE Trans. Pattern Anal. Mach. Intell. **13**(1), 813–819 (1991)
14. Otsu, N.: A threshold selection method from gray-scale histogram. IEEE Trans. Syst., Man C. **9**(1), 62–66 (1979)
15. Fieguth, P.W., Sinha, S.K.: Automated analysis and detection of cracks in underground scanned pipes. In: Proceedings of the 99th IEEE Image Conference, vol. 4, pp. 395–399 Kobe, Japan (1999)

Sunil K. Sinha received the Ph.D. degree in Civil Engineering and Systems Design Engineering from the University of Waterloo, Ontario, Canada, in 2000. Since 2001, he has been a Professor of Civil and Environmental Engineering at the Pennsylvania State University, PA, USA. He holds a joint appointment in the department of Computer Science and Engineering. He is also an Adjunct Professor of Systems Design Engineering at the University of Waterloo, Canada. His current research activities address problems in the areas of assessment technologies and decision-making methodologies for the rehabilitation of large-scale civil infrastructure systems, especially municipal infrastructure. He is a member of the ASCE, ASEE, ASTM, and NASTT.

Paul W. Fieguth received the B.A.Sc. degree from the University of Waterloo, Ontario, Canada, in 1991 and the Ph.D. degree from the Massachusetts Institute of Technology, Cambridge, in 1995, both degrees in electrical engineering. He joined the faculty at the University of Waterloo in 1996, where he is currently Associate Professor in Systems Design Engineering. He has held visiting appointments at the Cambridge Research Laboratory, at Oxford University and the Rutherford Appleton Laboratory in England, and at INRIA/Sophia in France. His research interests include statistical signal and image processing, hierarchical algorithms, data fusion, and the interdisciplinary applications of such methods. He is an active member of the IEEE.